Title

Planar patterned stretchable electrode arrays based on flexible printed circuits.

Journal

Journal of micromechanics and microengineering : structures, devices, and systems, 23(10)

ISSN

0960-1317

Authors

Taylor, RE
Boyce, CM
Boyce, MC
et al.

Publication Date

2013-10-01

DOI

10.1088/0960-1317/23/10/105004

Peer reviewed

Published in final edited form as:
J Micromech Microeng. 2013 October ; 23(10): . doi:10.1088/0960-1317/23/10/105004.

Planar patterned stretchable electrode arrays based on flexible printed circuits

R E Taylor[1], **C M Boyce**[2,3], **M C Boyce**[2,4], and **B L Pruitt**[1]

B L Pruitt: pruitt@stanford.edu

[1]Department of Mechanical Engineering, Stanford University, CA 94305 (USA)

[2]Infinite Corridor Technology, LLC, Winchester, MA 01890 (USA)

[4]Department of Mechanical Engineering, Massachusetts Institute of Technology, Cambridge, MA 02139 (USA)

Abstract

For stretchable electronics to achieve broad industrial application, they must be reliable to manufacture and must perform robustly while undergoing large deformations. We present a new strategy for creating planar stretchable electronics and demonstrate one such device, a stretchable microelectrode array based on flex circuit technology. Stretchability is achieved through novel, rationally designed perforations that provide islands of low strain and continuous low-strain pathways for conductive traces. This approach enables the device to maintain constant electrical properties and planarity while undergoing applied strains up to 15%. Materials selection is not limited to polyimide composite devices and can potentially be implemented with either soft or hard substrates and can incorporate standard metals or new nano-engineered conductors. By using standard flex circuit technology, our planar microelectrode device achieved constant resistances for strains up to 20% with less than a 4% resistance offset over 120,000 cycles at 10% strain.

1. Introduction

Robust, stretchable and conformal interconnects are necessary for the creation of stretchable electronics. To be ready for use in market devices, these interconnects must (1) be mechanically robust to cyclic stretch, (2) employ a robust manufacturing process, and (3) maintain stable electrical properties in the face of large cycle strains. Here we present a robust and planar stretchable electrode array with rationally designed perforations using standard materials and processing techniques.

Current stretchable electronic technologies have approached these goals, but no current technology has achieved all three: stretchable device robustness, manufacturing robustness and stable electrical properties. Wrinkled [1, 2], metal-on-elastomer as well as serpentine metal-in-elastomer and metal-polyimide-in-elastomer [3, 4] electrodes achieve repeatable large strains while maintaining electrical conductivity, but the fabrication process can be complex and highly variable. Further, the ultimate device properties often depend on initial substrate prestretch and/or metal deposition parameters. Great strides have been made with these platforms, some based on elastomer-embedded polyimide flex circuits, have withstood more than 500,000 cycles of stretch in fatigue testing [3, 5], but these rely on the elastomer support, which requires an encapsulation process that greatly increases thickness of the device and may introduce device property variations from time- and temperature-dependent

[3]Currently, Department of Chemical Engineering and Biotechnology, University of Cambridge, Cambridge CB2 1TN (UK)

elastomer stiffening. Additionally, making robust electrical connections between soft interconnects and circuit boards is nontrivial . These challenges as well as those of making multilayer devices are only beginning to be addressed [6, 7].

Undulating nanoribbon semiconductor structures harness planar microfabrication and standard materials, but also require the introduction of elastomers and a prestretch step [8–11]. These ribbons buckle out-of-plane, which can be limiting for applications that require contact and conformality, but nanoribbon designs do maintain nearly constant electrical properties while undergoing large strains. The primary applications for such devices include stretchable circuits and stretchable biosensors. A drawback of all wavy and wrinkle interconnect systems is their abrupt failure to open circuits, typically above fabrication prestretch strains of up to 50% [1, 10]. The emerging development and use of novel material systems such as stretchable conductive inks [12, 13], carbon nanotubes [14–17], or organic semiconductors [18, 19] provide a range of solutions to different challenges for stretchable electronics. However, these materials and their emerging manufacturing processes still limit their application outside of research labs. Typically two approaches have been taken to fabricate stretchable electronics: novel multi-scale materials to access nonlinear properties or novel manufacturing techniques to achieve new properties with standard materials [9]. Here, we present a robust, stretchable flex device that harnesses optimized perforated substrate geometries with both standard materials and processing techniques [20].

2. Results and Discussion

2.1. Rational Design Based on Finite Element Analysis

The Stretchable Micro-Electrode Array (SMEA) presented here was designed to fit a 4×4 array of electrodes with equidistant spacing in the vertical and horizontal directions. Device layout and layered construction are shown in supplementary figure S1. The array is 4.6 mm square with 305 μm square electrodes at 1.4 mm pitch and overall dimensions of 15.7 mm by 26.1 mm (figure 1A). The surrounding frame or “handle material” enabled the device to be handled easily in the laboratory without being damaged. To allow for uniaxial stretching in the horizontal direction, the SMEA was designed with a series of geometrically engineered perforations to the substrate, following the structured material substrates for flexible, stretchable electronics provided and practiced in Boyce et al. [21]. In brief, the substrate design provides for stretchable multi-layered electronic circuit boards through engineered perforations, which give low strain regions for component placement, vias, and interconnect routing. The result is both stretchable and conformal (figure 1B) and appropriate for both rigid and soft substrates ranging from elastomers up to hard polymers and even crystalline silicon. Conductors ranging from copper to nanowire meshes or organic conductors can also be incorporated into this type of stretchable composite. Here we use a flexible polymer substrate and common conductor to achieve ease of manufacture and our desired robustness to large strains.

Polyimide, with an elastic modulus of 2.5 GPa [22], is not easily stretched and must be modified to enable large elastic strains. The introduction of the engineered perforated geometry enables stretchability. The device is laser cut to create repeating segments of hinged regions that connect to relatively rigid islands (figure S1). In these perforated designs, certain designs are suitable for uniaxial strain only, while others are compatible with uni- and biaxial strains (see supplementary figure S2). The resulting device is flexible and stretchable enough to conform to surfaces of constant radius (figure 1B)

In this device, interconnects run through hinges to allow for a simple interface between the electrodes in the central columns and external electronic equipment (figure S1). When the electrode is stretched, the hinges remain planar and open up within the plane, allowing all of

the stretching to be undertaken in the hinge region, so that no strain is induced in the substrate region beneath the electrodes. The hinges are positioned following mirror symmetry about the center to eliminate any rotational motion of the rigid islands during stretching.

The hinge length, width, radius and thickness are designed to be within fabrication capabilities of flex circuit vendors and to favor in plane bending over out-of-plane twisting. Mechanical-only interconnects, without electrical connectivity, comprise the central column of hinges in figure S1. These mock interconnects ensure that all three columns of hinges have equivalent stiffness and will stretch equally, giving affine displacement of the columns of electrodes during stretching of the MEA.

A series of finite element analyses (ABAQUS) were undertaken to test and refine the perforation geometry. In these finite element analyses, the layers of polyimide, copper and adhesive were discretized (figure 1C), and macroscopic uniaxial strains up to 20% were applied to predict the resulting percentage of copper routing area below required in-plane strain thresholds (figure 1D), maximum principal in-plane strains in the metal (figure 1E) as well as out-of-plane rotation of the device (figure 1F). A sensitivity analysis was performed comparing three different candidate hinge designs that we will denote short, medium, and tall (referring to the relative lengths of the hinge arms). For all three designs, peak in-plane principal strains of the conductive interconnects were predicted to increase linearly with macroscopic applied strains, with taller hinges undergoing lower rates of increase (figure 1E). These peak strains occur over less than 1% of the interconnect width in the curved region of the hinge. The hinge design accommodates device strain primarily by the bending of the curved region and the rotation of the arms. At any given device strain, the tall hinge provides greater accommodation of strain by arm rotation and hence has lower strain in the conductive interconnects. All three designs were predicted to exhibit minimal out-of-plane rotation for macroscopic strains less than 17%, with rotation increasing dramatically at strains above 18%. Taller hinges were predicted to deform out-of-plane more than shorter hinges (figure 1F). This presented a design tradeoff to use the shortest hinges possible to minimize rotation while ensuring minimal device strains.

The elastic strain limit of copper on polyimide was used to guide this design decision, since plastic damage to the metal will compromise interconnect function. Copper alloys, like most metals, can undergo less than 1% strain elastically. Our 12.5 μm thick copper foil traces have a predicted yield stress of 220 MPa and Young's modulus of 110 GPa based on a model developed by Yu et al., who found that yield stress depends on copper thickness, not grain size, at this scale [23]. This model predicts a 0.2% elastic limit for our copper foil. For our uniaxial devices we targeted macroscopic elongations above 15%, while local strains remain below 1% in 99% of the device area and below 0.2% strain in at least 50% of the device. The short hinges could not meet these criteria, but our medium hinge designs did meet them (see figure 1D and table S1).

The medium hinge design (figure 1C) was fabricated using a laser cutting and laminating process (Altaflex, Santa Clara, CA). The device layer thicknesses are additional design parameters and can be used to tailor stiffness, provide a balance between in and out of plane deformation, and aid meet fabrication requirements. Simulations indicated that a thin device of 3 mil (75 μm) or less could maintain 15% strains without out-of-plane bending or in-plane strains much greater than 1%. For this reason we chose a 2 mil (50 μm) polyimide base layer with an integrated 0.5 mil (12.5 μm) high ductility copper foil trace layer followed by a 0.6 mil (15 μm) adhesive layer and finally a 0.5 mil (12.5 μm) cover film layer. The copper foil is patterned using laser direct imaging. A Yag laser with spot size of 20 μm, 25 μm entry beam width, and 355 nm wavelength laser rails was employed for cutting the polyimide

layers before lamination. A minimum trace-to-edge distance is enforced in design and fabrication; the copper traces are not laser cut but are patterned (this design and fabrication feature provides additional mechanical robustness to the traces since there are no edge defects from cutting). Bond pads for wirebonding are exposed on the top surface of the device, and a 4×4 array of microelectrodes is exposed through the bottom surface of the device. During through-thickness compression of device, the adhesive layer thickness decreased to 0.2 mil (5 μm). Table S2 in the Supplementary Material shows the materials and thicknesses used in our layered device fabrication. Finally, for surface biocompatibility, the device was electroplated with nickel and electrolytic hard gold to confine the exposed biostatic copper [24].

2.2. Mechanical and Electrical Testing

The resulting devices were electrically and mechanically tested to assess their mechanical strain characteristics and electrical robustness. Devices were stretched using a modified micromanipulation stage (ST-Japan) and a computer-controlled miniature linear actuator (Zaber T-LA60, Vancouver, BC, Canada). Imaging was performed using a USB microscope (Dino-Lite AM411T, AnMo Electronics, Taiwan) (see supplementary figure S4).

For stretching tests with concurrent electrical measurements, the stretchable microelectrode array devices were wirebonded to circuit boards (figure S5A). Electrodes along the rigid islands were thermocompression wirebonded together (figure S5B) to create current loops for electrical testing. All wirebonds were encapsulated in epoxy (5 Minute Epoxy, Devcon) for protection (figure S5C). Both linear actuator control and image analysis were performed in MATLAB using custom code. Four-point electrical measurements were performed with a source measurement unit (SMU-236, Keithley, Cleveland, OH) that was controlled remotely by MATLAB software via a GPIB connection with the KPIB MATLAB library.

Figure 2A shows finite element models of the entire array and images of a stretched device. Custom MATLAB software utilizing image cross correlations was used to extract electrode displacement from plan view device images. As predicted, the inter-electrode spacing remained uniform across the device and increased linearly with macroscopic uniaxial elongation (figure 2B). That is, the electrode array is expanding in the same manner expected for a solid elastomeric device. To test the electrical performance of the device a two-hinge current loop was created by wirebonding columns electrodes together (i.e., a daisy-chain of electrodes B1 through B4 as shown in figure S1) and four-wire (Kelvin) electrical measurements were performed across the terminating bond pads. A four-wire measurement was necessary because, unlike many stretchable interconnect systems, this system has extremely low-resistance traces of less than 1 Ω; this technique eliminates lead resistances from the measurement.

Throughout stepwise macroscale strains of up to 20%, the loop resistance remained constant (figure 2C). Further, fatigue testing of 5,000 cycles at 5% followed by 120,000 cycles at 10% strain demonstrated device robustness (figure 2D). The unstretched and stretched resistances were unchanged; however, over the course of 125,000 cycles the measured resistance increased by less than 4%. Since the pre- and post-experiment resistances remain the same, this 0.03 Ω increase is likely due to instrument offsets or temperature effects. For example, our source measure unit (Keithley 236) required a relatively high current of 10 mA to obtain 0.01 Ω measurement precision for our 1 Ω loops, implying 100 μW dissipated as heat. Most applications would not require such high currents. Regardless, the devices are robust at this level of power dissipation, throughout large strains and for high lifecycles.

We tested the out-of-plane behavior of the device by applying stretch and imaging the device from the side. We modified the MATLAB software used for displacement analysis to

extract island rotation information from these side view images (figure 3A). We performed cyclic strain testing at 5%, 10%, 15%, and 20% (figure 3BC). For strains up to 15% the observed rotation was minimal and in agreement with the finite element model (solid line). For strains above 15% the rotation dramatically increased. This finding was in general agreement with the simulation, but rotation occurred slightly earlier than the 17% predicted by finite element analysis. Figure 3C shows that if cyclic strain is kept to 15% or less, negligible rotation is observed.

Finally, thermal cycling was performed with a wirebonded device in a programmable environmental test chamber (Thermotron SM-1, Thermotron Industries, Holland, MI). From this cycling, the temperature coefficient of resistance of the device was experimentally measured to be 0.39 $°C^{-1}$ at 20 °C (supplementary figure S3). As expected, this matches the temperature coefficient of resistance of copper of 0.39 $°C^{-1}$. Therefore the 4% resistance change observed after 125,000 stretch cycles is on par with the resistance change observed with only a 10 °C temperature rise.

3. Conclusions

In addition to robust electromechanical performance, the following design and fabrication goals were met: 1) The devices are not fragile and can be manipulated without damage; 2) The simple fabrication process is compatible with established flexible printed circuit manufacturing, enabling future low-cost, mass production; 3) The device surfaces are made of biocompatible materials [25]; and 4) Electrical connection to the devices via conventional wirebonding is straightforward and robust. In comparison with many stretchable interconnect platforms that often fail abruptly as open-circuits, the failure mode of lost planarity in this device is preferable. Overstretched electrodes continue to function, but interconnects rotate out of plane linearly above 15% strain and trace resistances are minimally effected.

The geometries presented were limited only by the lithographic patterning, laser cutting, and alignment tooling of our flex device manufacturer. However, available manufacturing limits suggest that by narrowing traces and reducing trace-to-edge distances, we could manufacture arrays having two- to three-fold increased density of electrodes. Multiple traces can also be routed along the same hinges and further multi-layering is also easily possible using this approach. While the device presented here is designed for uniaxial stretch, other perforated geometry designs can be utilized for a biaxial straining and/or multi-axis curvature device (figure S2).

We have demonstrated the robustness of stretchable interconnects manufactured using conventional flexible circuit materials and processes. Such interconnects and devices can be engineered to maintain planarity and near-constant electrical properties throughout large cyclic strains. Further these devices maintain excellent electrical stability after more than a hundred thousand cycles at 10% strain. Applications such as stretchable electronics in textiles, stretchable photovoltaics, or stretchable biosensors are accessible not only because of the robust electromechanical properties enabled by our design, but also because of their manufacturability and the accessibility of standardized, low-cost production.

Supplementary Material

Refer to Web version on PubMed Central for supplementary material.

Acknowledgments

The authors thank C. Roozeboom for assistance with Thermotron oven programming, M. Hopcroft for KPIB assistance, P. Prather for wirebonding, and G. O'Brien for helpful discussions. This work was funded in part by NSF EFRI (MIKS-1136790), NIH R01 EB006745 and R33 HL089027, DARPA SBIR SB082-007, and Stanford DARE and BioX fellowships.

References

1. Lacour SP, Jones J, Suo Z, Wagner S. Design and performance of thin metal film interconnects for skin-like electronic circuits. Electron Devic. Lett. IEEE. 2004; 25:181.
2. Lacour SP, Wagner S, Huang Z, Suo Z. Stretchable gold conductors on elastomeric substrates. Appl. Phys. Lett. 2003; 82:2404–2406.
3. Verplancke R, Bossuyt F, Cuypers D, Vanfleteren J. Thin-film stretchable electronics technology based on meandering interconnections: fabrication and mechanical performance. J. Micromech. Microeng. 2012; 22:015002.
4. Jahanshahi A, Salvo P, Vanfleteren J. Reliable stretchable gold interconnects in biocompatible elastomers. J. Polym. Sci. Pol. Phys. 2012; 50:773–776.
5. Hsu Y-Y, Gonzalez M, Bossuyt F, Vanfleteren J, Wolf ID. Polyimide-Enhanced Stretchable Interconnects: Design, Fabrication, and Characterization. IEEE Trans. Electron Devic. 2011; 58:2680–2688.
6. Guo L, DeWeerth SP. High-Density Stretchable Electronics: Toward an Integrated Multilayer Composite. Adv. Mater. 2010; 22:4030–4033. [PubMed: 20717983]
7. Lin KL, Chae J, Jain K. Design and Fabrication of Large-Area, Redundant, Stretchable Interconnect Meshes Using Excimer Laser Photoablation and In Situ Masking. IEEE Trans. Adv. Packaging. 2010; 33:592–601.
8. Khang D-Y, Jiang H, Huang Y, Rogers JA. A Stretchable Form of Single- Crystal Silicon for High-Performance Electronics on Rubber Substrates. Science. 2006; 311:208–212. [PubMed: 16357225]
9. Rogers JA, Someya T, Huang Y. Materials and Mechanics for Stretchable Electronics. Science. 2010; 327:1607. [PubMed: 20339065]
10. Sun Y, Choi WM, Jiang H, Huang YY, Rogers JA. Controlled buckling of semiconductor nanoribbons for stretchable electronics. Nat. Nanotechnol. 2006; 1:201–207. [PubMed: 18654187]
11. Sun Y, Kumar V, Adesida I, Rogers JA. Buckled and Wavy Ribbons of GaAs for High-Performance Electronics on Elastomeric Substrates. Adv. Mater. 2006; 18:2857–2862.
12. Hyun-Joong K, Maleki T, Pinghung W, Ziaie B. A Biaxial Stretchable Interconnect With Liquid-Alloy-Covered Joints on Elastomeric Substrate. J. Microelectromech. S. 2009; 18:138–146.
13. Wei P, Taylor R, Ding Z, Chung C, Abilez OJ, Higgs G, Pruitt BL, Ziaie B. Stretchable microelectrode array using room-temperature liquid alloy interconnects. J. Micromech. Microeng. 2011; 21
14. Hu L, Pasta M, Mantia FL, Cui L, Jeong S, Deshazer HD, Choi JW, Han SM, Cui Y. Stretchable, Porous, and Conductive Energy Textiles. Nano Lett. 2010; 10:708–714. [PubMed: 20050691]
15. Lipomi DJ, Tee B CK, Vosgueritchian M, Bao Z. Stretchable Organic Solar Cells. Adv. Mater. 2011; 23:1771–1775. [PubMed: 21491510]
16. Lipomi DJ, Vosgueritchian M, Tee BCK, Hellstrom SL, Lee JA, Fox CH, Bao Z. Skin-like pressure and strain sensors based on transparent elastic films of carbon nanotubes. Nat. Nanotechnol. 2011; 6:788–792. [PubMed: 22020121]
17. Sekitani T, Nakajima H, Maeda H, Fukushima T, Aida T, Hata K, Someya T. Stretchable active-matrix organic light-emitting diode display using printable elastic conductors. Nat. Mater. 2009; 8:494–499. [PubMed: 19430465]
18. Lipomi DJ, Lee JA, Vosgueritchian M, Tee BCK, Bolander JA, Bao Z. Electronic Properties of Transparent Conductive Films of PEDOT:PSS on Stretchable Substrates. Chem. Mater. 2011; 24:373–382.

19. Vosgueritchian M, Lipomi DJ, Bao Z. Highly Conductive and Transparent PEDOT:PSS Films with a Fluorosurfactant for Stretchable, Flexible Transparent Electrodes. Adv. Funct. Mater. 2012; 22:421–428.

20. Taylor, RE.; Boyce, CM.; Boyce, MC.; Pruitt, BL. Proc. Microtechnologies in Med. and Biol. Marina del Ray, CA: 2013. Stretchable, Conformal Microelectrode Array Fabricated with Patterned Flex Circuit Technology.

21. Boyce MC, Socrate S, Boyce CM, Greviskes B. Structured Material Substrates for Flexible, Stretchable Electronics. U.S. Utility Patent Application. 2009; 12/822:609.

22. DuPont. DuPont Kapton polyimide film. Circleville, OH: 2012.

23. Yu DYW, Spaepen F. The yield strength of thin copper films on Kapton. J. Appl. Phys. 2004; 95:2991–2997.

24. Ghodssi, R.; Lin, P. Mems Materials, Processes Handbook. New York, USA: Springer-Verlag; 2010. Ch 3

25. Rousche PJ, Pellinen DS, Pivin DP Jr, Williams JC, Vetter RJ, Kirke DR. Flexible polyimide-based intracortical electrode arrays with bioactive capability. IEEE, T. Bio-med. Eng. 2001; 48:361–371.

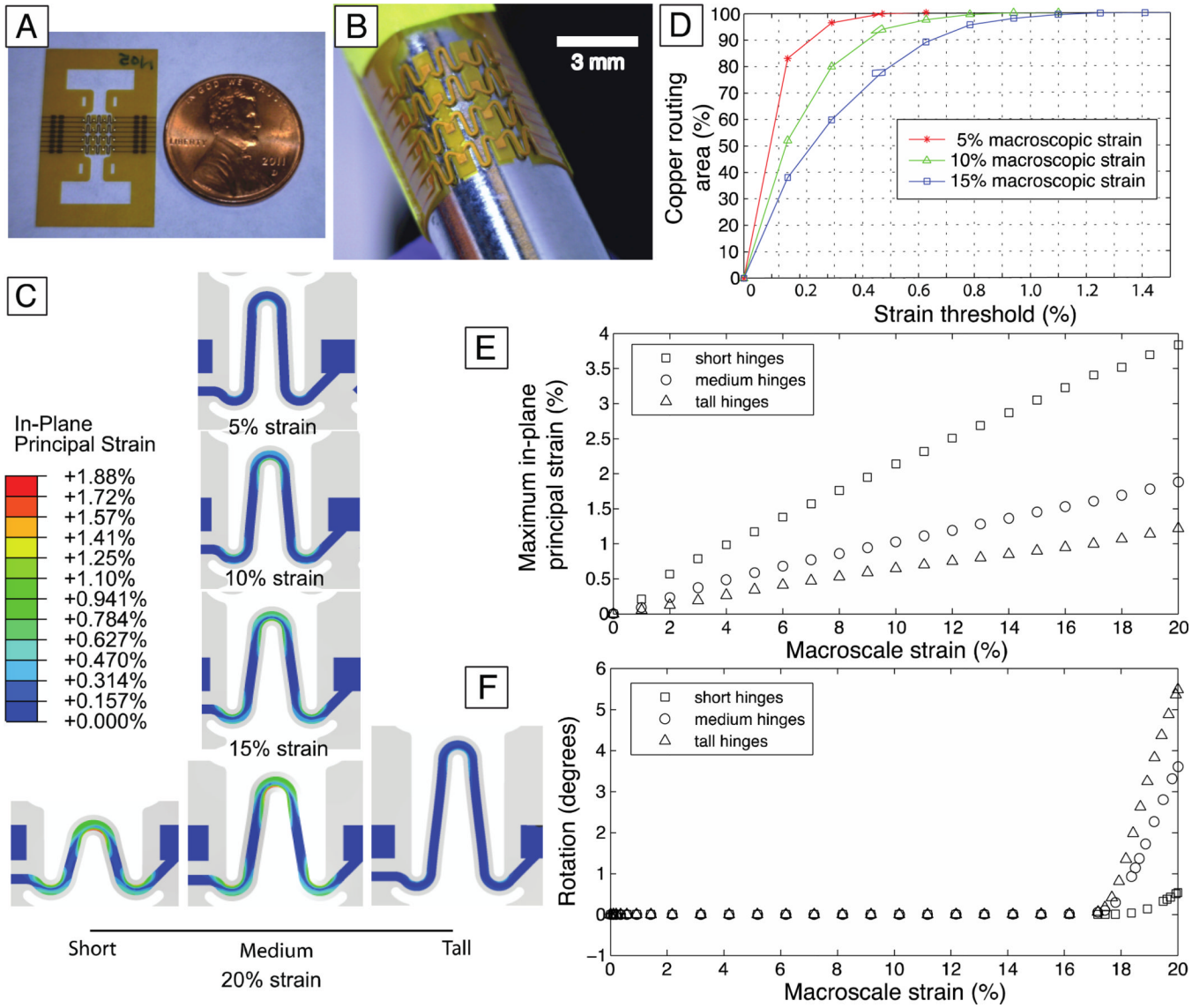

Figure 1.

(A) Array device (4×4 electrodes on rigid islands) with surrounding polyimide handle material is 15.7 mm wide by 26.1 mm long. The 4 × 4 electrode array region is 4.6 mm × 4.6 mm. (B) Device can conform to surfaces with a constant radius of curvature. Here the device is shown wrapped around a rod with 6 mm diameter. (C) Finite element simulations of a polyimide-copper device predict that in-plane principal strains in the metal layer are considerably lower than the macroscopic applied strain, with peak strains greater than 1% occurring only in the regions of highest curvature. (D) Copper routing area with microscopic in-plane strain less than various strain thresholds is plotted for 5%, 10%, and 15% macroscopic strain. In the medium hinges, less than 1% of the metal trace area is predicted to experience greater than 1% in-plane strain at macroscopic strains up to 15%. (E) Simulations predict that peak in-plane principal strains increase linearly with macroscopic strain, and the taller the hinges, the lower the peak strains. (F) Simulations predict that small, medium, and tall hinges will undergo minimal rotation at strains up to 17%, but at larger strains the out-of-plane rotation increases dramatically. Taller hinges experience more out-of-plane rotation.

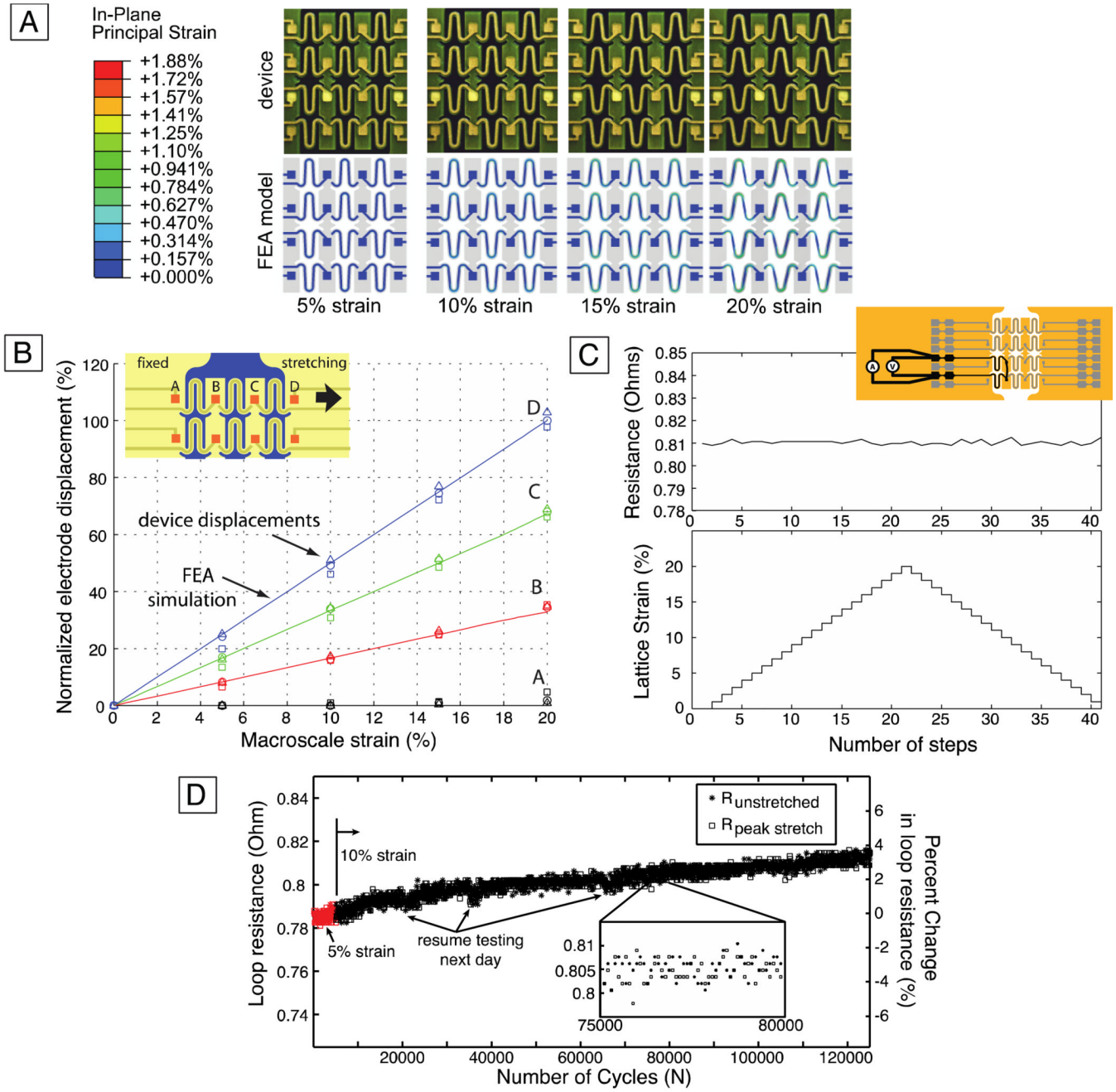

Figure 2.

Device stretch and electrical properties validate finite element modeling. (A) Actual stretch of device arrays (top row) agrees with predicted in-plane principal strain simulations (bottom row). (B) Electrode-to-electrode displacements for one row of electrodes for each of three devices were uniform and increased linearly with macroscopic applied strain as predicted by finite element model (solid line). (C) Throughout a cyclic strain test from 0% to 20% and back to 0% stepwise macroscopic strain, negligible change in loop resistance was observed. Eight electrical measurements were averaged for each point. (D) Throughout the course of 125,000 strain cycles (5,000 at 5% and 120,000 at 10%) the loop resistance increased by less than 4%.

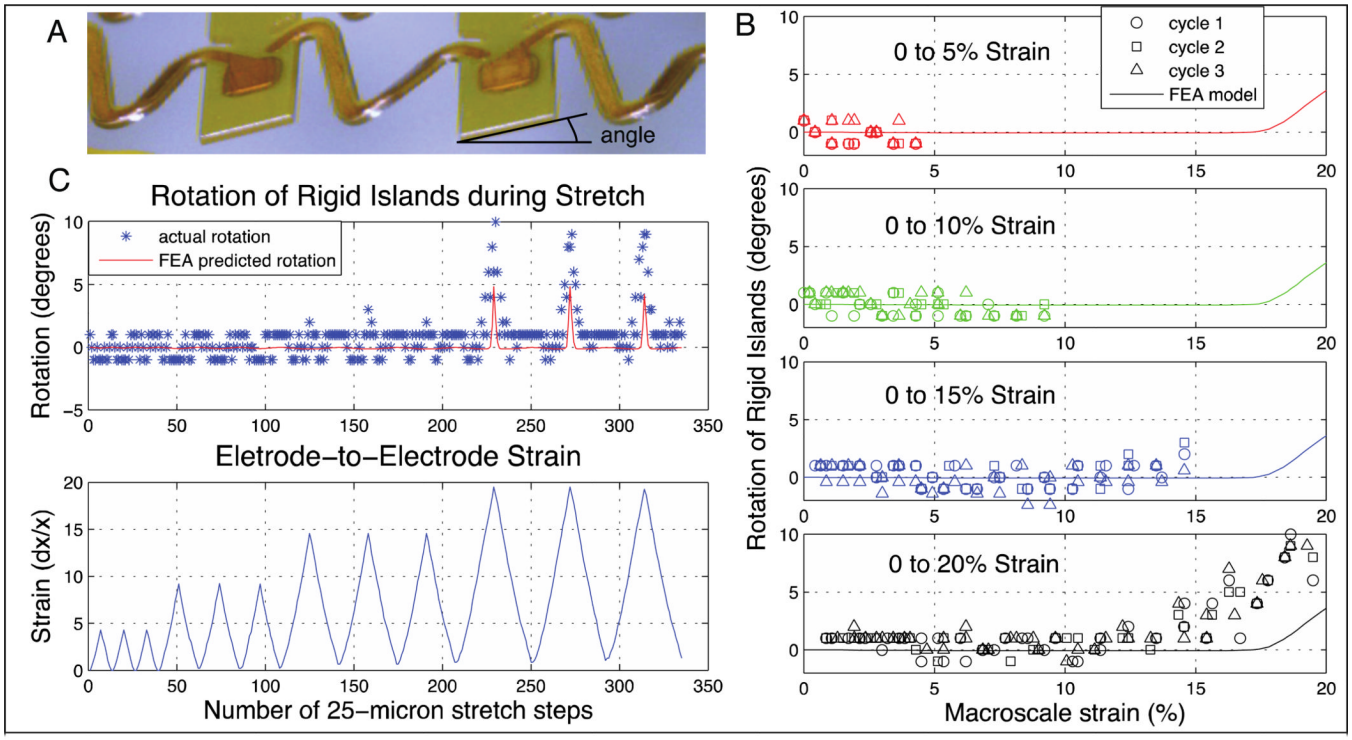

Figure 3.

(A) Out-of-plane motion was quantified as the angle of rotation of the island regions as demonstrated and labeled in this device detail image. (B) Throughout cyclic strains, the observed rotations largely agreed with the finite element simulations. For strains up to 15%, out-of-plane rotation was negligible, but the rotation quickly increased above 15%, slightly earlier than predicted by the simulation. (C) When subjected to sequential cyclic strains of 5%, 10%, 15%, and 20%, out-of-plane behavior was only observed between 15% and 20%, which generally agrees with the finite element predictions.